(This is a sample cover image for this issue. The actual cover is not yet available at this time.)

Journal of South American Earth Sciences 38 (2012) 57–70

Contents lists available at SciVerse ScienceDirect

Journal of South American Earth Sciences

journal homepage: www.elsevier.com/locate/jsames

Metamorphic evolution of the Río de la Plata Craton in the Cinco Cerros area, Buenos Aires Province, Argentina

Hans-Joachim Massonne [a,*], Jorge A. Dristas [b], Juan Cruz Martínez [c]

[a] Institut für Mineralogie und Kristallchemie, Universität Stuttgart, Azenbergstrasse 18, D-70174, Germany
[b] CIC, INGEOSUR and Departamento de Geología, San Juan 670, UNS, Bahía Blanca 8000, Argentina
[c] CONICET-INGEOSUR and Departamento de Geología, San Juan 670, UNS, Bahía Blanca 8000, Argentina

ARTICLE INFO

Article history:
Received 7 June 2011
Accepted 18 May 2012

Keywords:
Río de la Plata Craton
Metamorphic evolution
Garnet
Metapelite
P–T pseudosection
Geodynamics

ABSTRACT

A metapelite and an interlayered granite were studied from the Cinco Cerros area ca. 65 km WNW of the city of Mar del Plata. Garnet in these samples is slightly zoned with core and rim compositions of $pyr_{17}(gro + andr)_6spes_{1.5}alm_{75.5}$ and $pyr_{13.5}(gro + andr)_{5.5}spes_2alm_{80}$, respectively, in the metapelite. Corresponding compositions in the granite are $pyr_{15}(gro + andr)_{3.5}spes_{3.5}alm_{78}$ and $pyr_{11}(gro + andr)_{3.5}spes_{4.5}alm_{81}$. We used the PERPLE_X computer software package to calculate *P–T* pseudosections. From the pseudosection of the metapelite *P–T* conditions of 6.7 kbar and 670 °C were derived for an early metamorphic stage. Subsequently, a pressure release occurred at decreasing temperatures. The final metamorphic *P–T* conditions recorded by the studied rock are 4.5 kbar and 600 °C compatible with the absence of cordierite, staurolite, and an Al_2SiO_5-phase. Garnet in the granitoid crystallized between 715 and 690 °C at a pressure around 7.7 kbar.

U–Th–Pb age dating with the electron microprobe was performed. 16 analyses of monazite in the metapelite formed three clusters resulting in ages of I: 2073 ± 11.4 (1σ) Ma, II: 1913 ± 11.0 (1σ) Ma, and III: 1805 ± 20.8 (1σ) Ma. Thus, the Paleoproterozoic metamorphic event can be related to the Trans-Amazonian cycle and was followed by slow cooling.

As our study area is close to the margin of the Río de la Plata Craton, where abundant magmatic arc-derived plutonic rocks are outcropping, we interpret the derived *P–T* data as follows: A heating event (not recorded by the studied rocks) resulted from magmas that intruded during the Trans-Amazonian cycle. This event was followed by slow exhumation, probably caused by erosion, accompanied by thermal relaxation.

1. Introduction

The evolution of the old cratonic areas on Earth can only be understood in the full context of petrological, geophysical, and geochemical including geochronological data. The former data, leading to reasonably well derived pressure–temperature (*P–T*) paths for metamorphic rocks, are, thus, capable to constrain geodynamic models for collisional settings older than 1 billion years. Basic work in this respect was undertaken, for instance, by Bohlen and Mezger (1989) demonstrating that old granulite terranes experienced pressures usually between 6 and 8 kbar and are, thus, typical for the middle orogenic crust in ancient times. For some cratons petrological work, leading to data of the *P–T* evolution of rocks, is nearly lacking despite numerous attempts to fully understand the evolution of corresponding cratonic regions nearly without such data. This is also the case for the Paleoproterozoic Río de la Plata Craton in South America (see below). For this reason, we decided to enhance the petrological and *P–T–t* evolutionary knowledge of this craton by the study of a small exposure of basement rocks in Argentina, the Cinco Cerros area.

2. Geological setting

2.1. Río de la Plata Craton and Tandilia belt

The Río de la Plata Craton (RPC), occurring in the southeastern part of the South American plate (Fig. 1), is one of several cratons that are part of this plate. The RPC itself is assembled by a group of ancient continental blocks, terranes and belts outcropping in Uruguay and the central-eastern part of Argentina with possible additional fragments in southern Brazil and Paraguay (compare Bossi and Cingolani, 2009; Oyhantçabal et al., 2011; Tohver et al.,

* Corresponding author. Tel.: +49 711 68581225; fax: +49 711 68581222.
E-mail address: h-j.massonne@mineralogie.uni-stuttgart.de (H.-J. Massonne).

0895-9811/$ – see front matter © 2012 Elsevier Ltd. All rights reserved.
doi:10.1016/j.jsames.2012.05.005

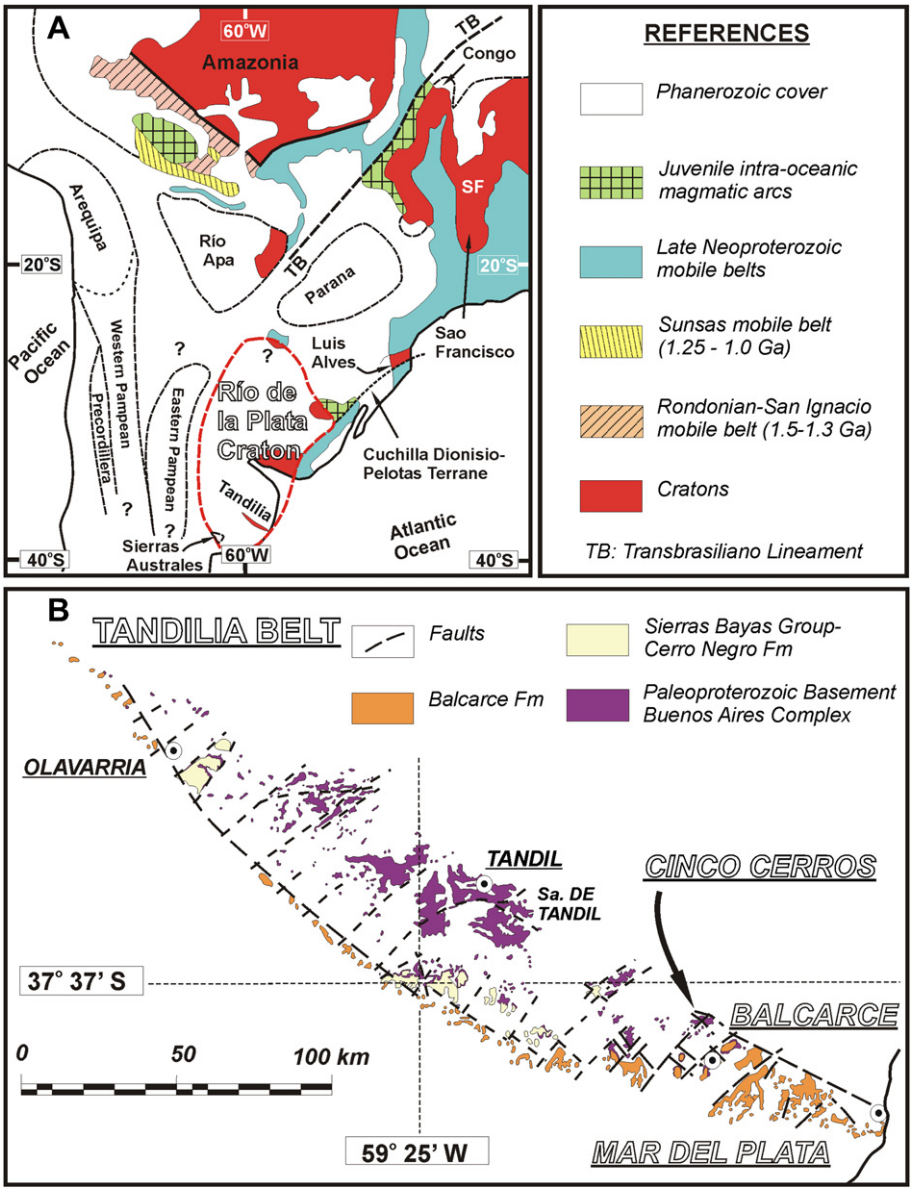

Fig. 1. (A) Schematic Precambrian tectonic framework of central South America modified after Cordani et al. (2003), Kröner and Cordani (2003), Rapela et al. (2007), Oyhantçabal et al. (2011), and Tohver et al. (2012). Dashed lines indicate inferred positions of major cratonic fragments below the Phanerozoic cover. (B) Geological map of the Tandilia belt modified after Iñiguez (1999) and Poiré and Spalletti (2005).

2012). However, the relations of these outcropping fragments are not very clear because considerable parts of the RPC are covered by younger sediments that were partially involved in the Brazilian orogeny during the assembly of Gondwana (e.g. Rapela et al., 2007, 2011). This orogeny also led to reworking of basement crust at the eastern margin of this craton (e.g. Basei et al., 2011). The group of continental blocks within the RPC is dominated by juvenile Paleoproterozoic rocks with restricted Archean domains (Rapela et al., 2007). Among them the Tandilia belt in Argentina is usually mentioned as a southern outcrop region of the RPC (Cingolani et al., 2002; Pankhurst et al., 2003; Dalla Salda et al., 2005).

The Tandilia belt in the central part of the Buenos Aires Province is a northwest to southeast trending, 350 km long and up to 60 km wide complex (Fig. 1). The basement of this belt consists of igneous–metamorphic rocks dominated by granitic to tonalitic gneisses, migmatites, and granitoids with scarce schist, marbles, amphibolites, and ultramafic rocks grouped in the Buenos Aires Complex (BAC; Di Paola and Marchese, 1975). The western and southwestern rocks of the BAC are unconformably overlaid by subhorizontal Neoproterozoic to Early Paleozoic shallow marine siliciclastic and carbonatic sedimentary rocks (Dalla Salda and Iñiguez, 1979; Iñiguez et al., 1989). This sedimentary succession is called the La Tinta Formation (Leveratto and Marchese, 1983) or the Sierras Bayas Group plus the Cerro Negro and Balcarce formations (Poiré and Spalletti, 2005).

The evolution of the basement of the Tandilia belt is mainly related to the Trans-Amazonian cycle, ca. 2.2–1.8 Ga (Cingolani and Dalla Salda, 2000; Cingolani et al., 2002, 2005; Hartmann et al., 2002; Pankhurst et al., 2003; Cingolani, 2011). According to Hartmann et al. (2002) two Paleoproterozoic orogenies, identified by U–Pb SHRIMP geochronology on zircon, can be correlated with the accretionary Encantadas orogeny (2.25–2.12 Ga) and the collisional Camboriu orogeny (2.10–2.08 Ga) which occur along a considerable part of the Brazilian shield. Besides, Sm–Nd model

ages of crustal material point to Neoarchean sources likewise in other portions of the southern Brazilian shield (Cingolani et al., 2002; Hartmann et al., 2002; Pankhurst et al., 2003). Extended mylonite belts occurring shortly after the intrusions of granitoids during the Trans-Amazonian cycle (Cingolani et al., 2002) overprinted these rocks by metamorphic conditions of the lower greenschist to amphibolite facies (Frisicale et al., 2001, 2005). Two suites of calc–alkaline and tholeiitic dike swarms originated from depleted to incompatible elements-enriched mantle sources and were emplaced during the transtensional to post-collisional stages of the Trans-Amazonian Cycle (Iacumin et al., 2001; Texeira et al., 2002). In the Tandilia belt, the only rocks related to the Brazilian orogenic cycle (ca. 600 Ma), drilled at the easternmost belt near the city of Mar del Plata (Marchese and Di Paola, 1975), are equivalents to those exposed in the igneous–metamorphic belt in eastern Uruguay (Rapela et al., 2011).

Different collisional models were proposed to explain the metamorphic evolution of the Tandilia belt (Teruggi et al., 1988; Ramos et al., 1990; Dalla Salda et al., 1992; Ramos, 1999; Cingolani, 2011). A model of continent–continent collision, to which the extended shear belts were related to, was argued by Dalla Salda et al. (1992) in an attempt to explain the formation of anatectic leucogranites during a second deformational event. Another model of continent–continent collision hypothesized the collision of the allochthonous terrane of Tandilia with the Río de la Plata Craton. Portions of oceanic crust, related to local outcrops of oceanic crust consisting of metacherts, metagreywackes and metabasalts, were attached and metamorphosed at low greenschist facies (Teruggi et al., 1988) during this collision. Taking into account such basic volcanics, Ramos et al. (1990) proposed the existence of an island arc that was trapped between the Río de la Plata Craton and the Tandilia terrane when these blocks finally collided at 1.8 Ga.

2.2. The Cinco Cerros – Balcarce area

Several basement areas are exposed in the Tandilia ranges. The one of the Cinco Cerros (=five peaks) is located ca. 65 km WNW of the city of Mar del Plata (Fig. 1). This basement area is supplemented by basement at the town of Balcarce where metamorphic rocks, derived from a sedimentary stratified sequence, were reported including gneisses, migmatites, amphibolites and scarce dolomitic marbles and schists (Teruggi et al., 1974; Cortelezzi et al., 1999; Delpino and Dristas, 2008). At Balcarce, granitic to tonalitic gneisses and migmatites are commonly garnet-bearing with quartz, plagioclase and/or microcline-rich leucosomes. Mafic minerals include biotite, amphibole and occasionally pyroxene (clinopyroxene and/or orthopyroxene). Orthopyroxene-bearing and amphibolitic granulites at the El Triunfo hill of Balcarce (Delpino, 2000) were dated with a SHRIMP (U–Pb in zircons) as 2196 ± 4 Ma by Cingolani et al. (2002). These authors determined a similar U–Pb age of 2194 ± 5 Ma for a migmatitic gneiss cropping out in a quarry at the side of road 226 about 12 km NNW of Balcarce, whereas an age of 2176 Ma was obtained from a garnet-bearing gneiss of the Punta Tota – Bachicha hill (Cingolani et al., 2002; Hartmann et al., 2002) at road 226 close to the Balcarce main access. A significant younger zircon U–Pb SHRIMP age of 2073 Ma ± 6 Ma was reported for an anatectic garnet-bearing tonalite intruded in migmatitic gneisses at the side of the road 226 about 11 km NNW of Balcarce (Cingolani et al., 2002; Hartmann et al., 2002). These migmatites are very similar to those outcropping in the Cinco Cerros area (Dalla Salda et al., 2006).

Delpino and Dristas (2008) investigated the metamorphic evolution of dolomitic marbles and associated calc–silicate rocks from Punta Tota – Bachicha hill, through petrographic, geothermobarometric and fluid inclusion studies. These authors concluded that thin dolomitic marbles were intercalated within amphibolites forming the upper part of a stratified basement showing biotite–garnet gneisses overlaying migmatites with profuse pegmatitic segregates at the base. The estimated *P–T* metamorphic conditions were of 750–800 °C and 5–6 kbar, followed by near isobaric cooling to about 500–450 °C and 5.5–6.5 kbar suggesting a counter-clockwise path. The pressure conditions of 6 kbar and more are confirmed by a few works applying geothermobarometry on rocks of the Tandilia belt (Frisicale et al., 2005, 2010, 2012: 6–9 kbar for the Azul megashear zone) and other basement outcrops of the RPC (Hartmann, 1998: 800 °C and 10 kbar; Massonne et al., 2001: early stage 9 kbar and 800 °C, late-stage 7 kbar and 700 °C for the Santa Maria Chico Complex). For the Punta Tota area, Delpino and Dristas (1999) proposed in situ anatexis for the migmatites at granulite facies conditions. According to these authors, the biotite-dehydration reactions in tonalitic paragneisses gave rise to widespread migmatization and the formation of scarce granulites (two pyroxene granulites), interpreted as anatectic restites.

3. Location and description of relevant samples

The Cinco Cerros area (Fig. 2), ca. 11 km north of Balcarce, is characterized by steeply dipping gneisses, migmatites, amphibolites and banded meta-igneous rocks (60°–90°) with an ENE trending main structure (S_1) coincident with previous stratification (S_0). Profuse leucocratic quartz–K-feldspar-bearing segregates are mainly concordant with the S_1 structure and folded by F_2. Lenses of amphibolites and ultramafic rocks (pyroxenites) are rarely interbedded in the sequence.

Gneisses (studied samples 03181109, 05181109, 06181109, 07181109, 08181109 from site 1 – see Fig. 2; 04180410, 05180410, 06180410 from site 3; 08180410 – site 4, 01190410 – site 6, 05190410 – site 9) are the dominant rock type in the Cinco Cerros area. These rocks are well-foliated, grey to red colored and composed of quartz, plagioclase, and biotite. Occasionally, garnet, amphibole or K-feldspar can be present. Plagioclase and quartz are granoblastic with evidence of internal recrystallization. Myrmekitic textures were observed at recrystallized rims of plagioclase porphyroblasts. Reddish to brown pleochroic laths of biotite, partly recrystallized and chloritized, define the main foliation (S_1). Garnet porphyroblasts, as large as 1.5 cm, are usually poikilitic with inclusions of quartz, biotite, plagioclase and rare amphibole, opaque phase, apatite, and monazite. Accessories in the gneisses are zircon, ilmenite, apatite and monazite. Transitional to gneisses, migmatites (sample 09181109 – site 2, 12181109 – site 8, 03190410 – site 7) are characterized by well-banded leucocratic segregates with abundant K-feldspar (microcline) and less biotite. Unless litpar-lit structures are seen, the migmatites can hardly be differentiated from meta-igneous banded bodies.

Amphibolites usually display a nematoblastic to granoblastic texture with variable contents of plagioclase. They are (sample 10181109 from site 2, 07180410 – site 4) mainly composed of amphibole, plagioclase, and biotite. Occasionally quartz appears as granoblastic grains, commonly included in plagioclase and amphibole, in these rocks. Plagioclase in amphibolites, as well as in gneisses with amphibole (sample 011904 from site 6), is completely replaced by K-white mica, calcite and zoisite–clinozoisite. Biotite laths are bended and retrogressed to chlorite and zoisite–clinozoisite. Accessories are opaque minerals, apatite and zircon. The ultramafic rocks are pyroxene-rich and plagioclase-free granular rocks. Oikocrysts of orthopyroxene as large as 1 cm include amphibole, biotite and FeAl–spinel.

We studied two rock types from sample site 1 (Fig. 2) in very detail. Sample 01181109 is from a meter-thick garnet-bearing

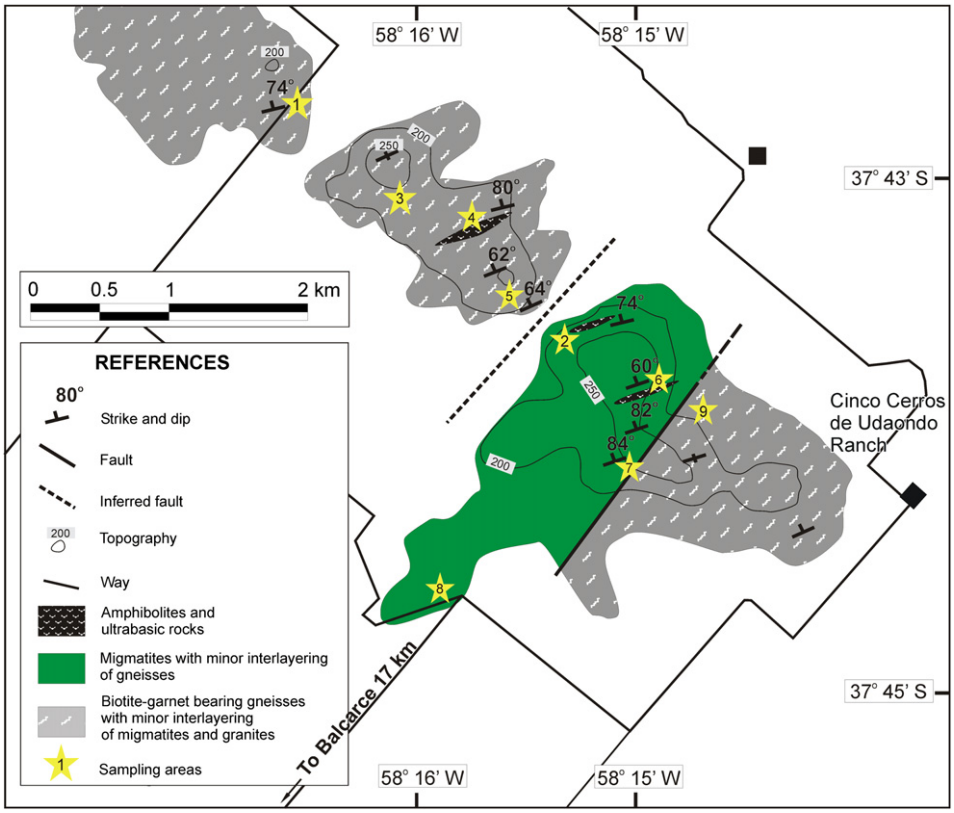

Fig. 2. Geological information on and sample locations, indicated by stars, in the Cinco Cerros area. For provenance of specific samples: see text.

granite which is interlayered in a gneiss. This sample contained mm-sized quartz, K-feldspar and plagioclase before slight deformation and mineral alteration (therefore, we call the rock "altered granite" in the following). Igneous Fe–Mg-bearing minerals were biotite and garnet. The latter mineral can be easily recognized with the naked eye by reddish, homogeneously distributed grains up to a few millimeters in diameter appearing in the whitish quartz–feldspar matrix. The content of garnet in the rock is about 2 vol.%. Biotite made up a similar content in the granite once but is now completely altered to chlorite + minor Ti-bearing opaque phase. Muscovite is an accessory phase that can form up to 1 mm-sized grains with irregular shape (Fig. 3). As it often appears along grain boundaries of feldspars, muscovite was either formed as late-magmatic mineral or by replacement of feldspars at subsolidus conditions. Possibly both processes could have taken place. Fine-grained white mica (sericite) is rarely replacing plagioclase. A deformation event resulted in recrystallization of quartz and occasional fracturing of K-feldspar.

Sample 06181109 is from a dark grey, biotite- and garnet-rich gneiss. These mafic minerals make up 15–20 vol.% and 10–15 vol.%, respectively, of the rock. Ilmenite (1 vol.%) is the opaque phase. Contents of plagioclase are in the range of 20–25 vol.%. In fact, oriented biotite and garnet are enriched in layers (see Fig. 3D) but any signs of true leucosomes are lacking. Thus, in contrast to migmatites in the vicinity of sample site 1, the biotite- and garnet-rich gneisses were not molten.

4. Methods

Mineralogical and textural observations were made through a polarizing microscope. Chemical compositions of minerals, including X-ray mapping, were acquired by a CAMECA SX100 electron microprobe (EMP) equipped with five wavelength-dispersive spectrometers. Beam current and acceleration voltage were 15 nA and 15 kV, respectively. A slightly defocused beam was used. Counting times to obtain the concentrations of F, Na, Mg, Al, Si, Cl, K, Ca, Ti, Cr, Mn, Fe, and Ba were 20 s at the corresponding Kα (Lα for Ba) peak and on the background except for F (30 s). Natural and synthetic standards were adopted for the calibration of the EMP. X-ray maps were prepared by stepwise movement (every 100 ms) of the thin section under the electron beam (50 nA) of the microprobe and subsequent computer-aided evaluation.

Bulk-rock analyses were undertaken with a PHILIPS PW2400 X-ray fluorescence (XRF) spectrometer. For this purpose, finely ground rock powder, obtained with a WC dish-and-puck mill, was fused with Spectromelt® (ratio 1:9) to prepare glass disks used for the analyses of major elements.

In order to derive *P–T* paths for the two selected rocks we focussed on the calculation of *P–T* pseudosections for fixed rock compositions. For these calculations, the computer program package PERPLE_X (Connolly, 1990 – version downloaded from http://www.perplex.ethz.ch, August 17, 2006), mainly thermodynamic data for mineral end-members and H_2O given by Holland and Powell (1998, updated in 2002), and the following solid-solution models (see Holland and Powell, 1996, 1998; Powell and Holland, 1999) were applied: GlTrTsPg for amphibole, TiBio(HP) for biotite, Chl(HP) for chlorite, hCrd for cordierite, Ep(HP) for clinozoisite–epidote, Gt(HP) for garnet, IlGkPy for ilmenite, Opx(HP) for orthopyroxene, Pheng(HP) for potassic white mica and St(HP) for staurolite (newest_format_solut.dat). The used models for feldspars (plagioclase and K-feldspar), paragonite (model Pa(M)), Na-rich clinopyroxene (model Acm(M)) and Ti-bearing magnetite (model Usp(M)) were reported by Massonne and Willner (2008) and Massonne (2010, 2011). In addition, the

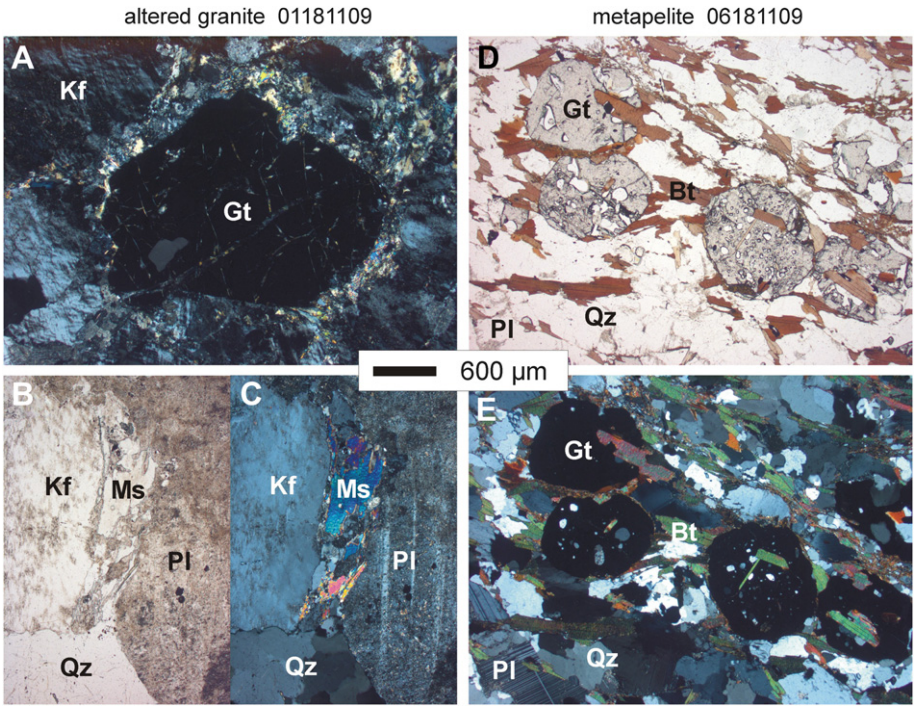

Fig. 3. Photomicrographs of objects in the studied altered granite and metapelite seen under plane-polarized light (B,D) and under crossed nicols (A,C,E). Abbreviations: Bt = biotite, Gt = garnet, Kf = K-feldspar, Ms = muscovite, Pl = plagioclase, Qz = quartz.

model melt(HP) for haplogranitic melt (White et al., 2001, 2003) was used.

The calculations with PERPLE_X were undertaken in the system Na_2O–K_2O–CaO–FeO–O_2–MnO–MgO–Al_2O_3–SiO_2–TiO_2–H_2O. For this purpose, the bulk-rock analyses obtained with the XRF spectrometer were somewhat simplified (Table 1). The O_2 contents of these simplified bulk-rock compositions were estimated assuming 7% (altered granite) and 5% (metapelite) of the iron being trivalent. Contents of H_2O were assumed to be 1 wt% and 3.5 wt%. At the first glance, the latter value seems to be too high for metapelites adjacent to migmatites but such high H_2O contents were derived to be stored in similar metapelites from the anatectic Ulten zone in Southern Tyrol (Braga and Massonne, 2012). In reconnaissance calculation runs the compositional range of the relevant solid-solutions were explored so that for a final run these ranges could be correspondingly reduced and the resolutions enhanced approaching the maximum number of one million pseudo-component compounds. With specific sub-programs (werami, pscontor) of PERPLE_X contoured *P*–*T* graphs were also produced which are related to molar fractions of garnet and Si pfu in phengite. The curves in all graphs were smoothed according to Connolly (2005).

In addition to the PERPLE_X calculation we used conventional geothermometry to gain access to metamorphic *P*–*T* conditions of the Cinco Cerros rocks. For this purpose the Fe^{2+}–Mg exchange thermometry for the garnet–biotite pair was applied using the empirical calibration by Kleemann and Reinhardt (1994; THERBARO program: Kleemann, unpubl.).

Table 1
Bulk-rock compositions of altered granite 01181109 and metapelite 06181109 from the Cinco Cerros area determined with XRF spectrometry. The simplified compositions (see text) were used for calculations with the computer software PERPLE_X.

Sample no.	01181109	06181109	01181109 simplified	06181109 simplified
SiO_2	76.238	59.998	76.389	58.958
TiO_2	0.000	1.066	0.000	1.048
Al_2O_3	13.127	15.558	13.153	15.288
Fe_2O_3	1.528	13.469		
FeO			1.378	11.910
O_2			0.010	0.066
MnO	0.063	0.187	0.063	0.184
MgO	0.150	2.867	0.150	2.817
CaO	0.760	2.621	0.742	2.284
Na_2O	3.210	2.039	3.216	2.004
K_2O	3.891	1.975	3.899	1.941
P_2O_5	0.015	0.225		
H_2O			1.000	3.500
Sum	98.980	100.005	100.000	100.000

5. Results

5.1. Mineral compositions

The compositions of garnet in both samples are slightly variable as can be seen in the X-ray maps of Fig. 4. In case of the altered granite, garnet core compositions are characterized by about 15 mol % pyrope and 3.5 mol% spessartine and grossular + andradite components each (=pyr_{15}(gro + andr)$_{3.5}$$spes_{3.5}$$alm_{78}$, Table 2). Towards the rim, the Ca contents in garnet slightly increase whereas the Mg and Mn contents significantly decrease and increase, respectively (Fig. 5). The rim composition of garnet in sample 01181109 is pyr_{11}(gro + andr)$_{3.5}$$spes_{4.5}$$alm_{81}$ (Table 2). In the biotite gneiss 06181109 the core composition of garnet is pyr_{17}(gro + andr)$_6$$spes_{1.5}$$alm_{75.5}$. Towards the rim, slightly increasing Mn contents and significantly decreasing Mg contents were observed (Fig. 6). Contents of Ca first decreased and then increased reaching a rim composition of $pyr_{13.5}$(gro + andr)$_{5.5}$$spes_2$$alm_{80}$.

Relatively large grains of muscovite in the altered granite are slightly inhomogeneous in composition. Contents of Si range between about 3.05 and 3.14 per formula unit (pfu). These contents above that of ideally composed muscovite (Si = 3.00 pfu) are due to

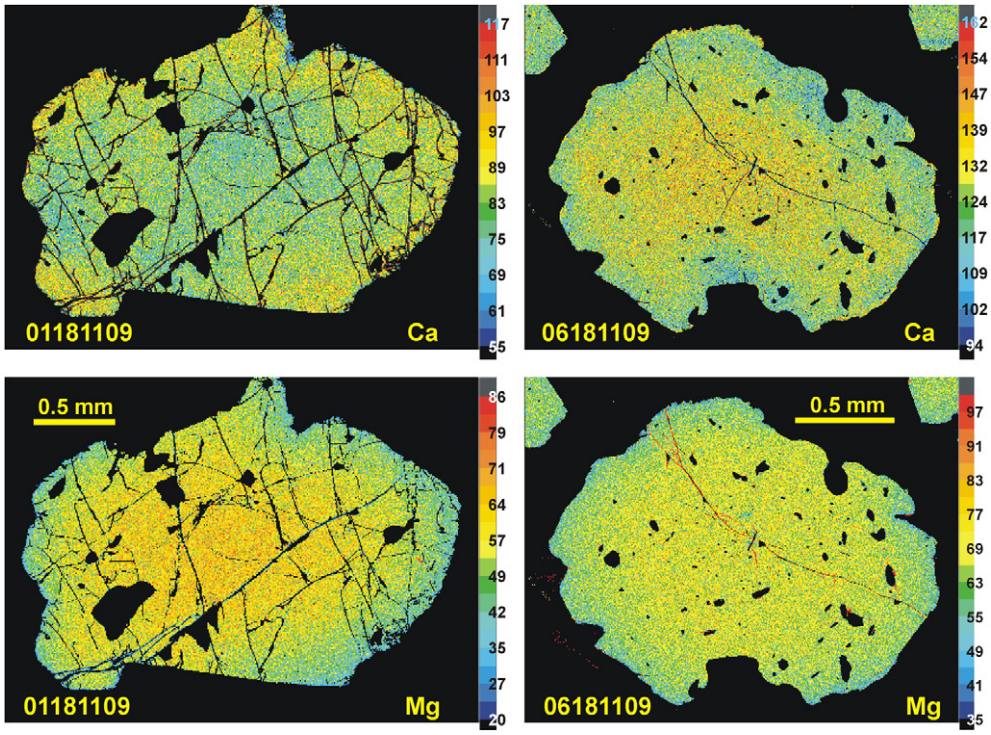

Fig. 4. Ca and Mg concentration maps obtained with a CAMECA SX100 electron microprobe of garnet from altered granite sample 01181109 and metapelite 06181109. The color code on the right hand side of each image is related to counts per second.

Table 2
EMP analyses of minerals in the studied altered granite (01181109) and metapelite (06181109). Structural formulae were calculated on the following basis: garnet: 24 O, 10 six- and eight-fold coordinated cations; muscovite: 42 − (Ca + Ba) valencies; biotite: 21 valencies; feldspars: 5 cations; ilmenite: 6 valencies, 2 cations.

Sample	01181109					06181109				
Mineral	Garnet core	Garnet rim	Muscovite	Plagioclase	K-feldspar	Garnet core	Garnet rim	Biotite	Plagioclase	Ilmenite
Anal.-No.	306-2	306-14	308-13	308-42	308-36	306-37	306-18	305-3	305-28	308-5
SiO_2	37.91	37.59	47.10	67.87	65.06	38.10	37.84	35.81	60.39	
TiO_2	0.00	0.00	0.17	0.01	0.01	0.09	0.00	3.47	0.00	52.38
Al_2O3	21.66	21.68	36.49	20.62	18.57	21.73	20.97	17.88	24.86	0.00
Cr_2O_3	0.03	0.00	0.01	0.00	0.00	0.04	0.03	0.10	0.01	0.02
Fe_2O_3	0.42	0.13		0.00	0.03	0.49	0.83		0.00	1.68
FeO	36.03	37.30	0.94			35.26	35.92	18.89		46.59
MnO	1.59	2.14	0.00	0.00	0.02	0.76	0.96	0.00	0.00	0.40
MgO	4.01	2.75	0.46	0.00	0.01	4.41	3.52	10.20	0.00	0.07
CaO	1.23	1.24	0.00	0.98	0.00	2.15	1.76	0.00	7.11	
Na_2O	0.01	0.02	0.42	11.25	0.34	0.00	0.03	0.16	7.49	
K_2O			11.18	0.09	16.42			9.80	0.18	
BaO			0.17	0.02	0.55			0.19	0.01	
F			0.00					0.26		
H_2O calc			4.58					3.86		
Sum(cor)	102.88	102.86	101.52	100.84	101.01	103.01	101.86	100.51	100.06	101.14
Si	5.863	5.863	6.165	2.947	2.990	5.860	5.969	2.697	2.688	
Ti	0.000	0.000	0.016	0.000	0.000	0.011	0.000	0.197	0.000	0.984
Al	3.948	3.985	5.628	1.055	1.006	3.939	3.898	1.587	1.304	0.000
Cr	0.003	0.001	0.001	0.000	0.000	0.004	0.004	0.006	0.001	0.000
Fe	4.708	4.879	0.103	0.000	0.001	4.592	4.835	1.190	0.000	1.005
Mn	0.208	0.282	0.000	0.000	0.001	0.099	0.128	0.000	0.000	0.008
Mg	0.925	0.639	0.091	0.000	0.000	1.012	0.827	1.145	0.000	0.003
Ca	0.203	0.208	0.000	0.046	0.000	0.354	0.297	0.000	0.339	
Na	0.003	0.007	0.108	0.947	0.030	0.000	0.010	0.024	0.646	
K			1.867	0.005	0.963			0.942	0.010	
Ba			0.009	0.000	0.010			0.005	0.000	
F			0.000					0.061		
H			4.000					1.939		

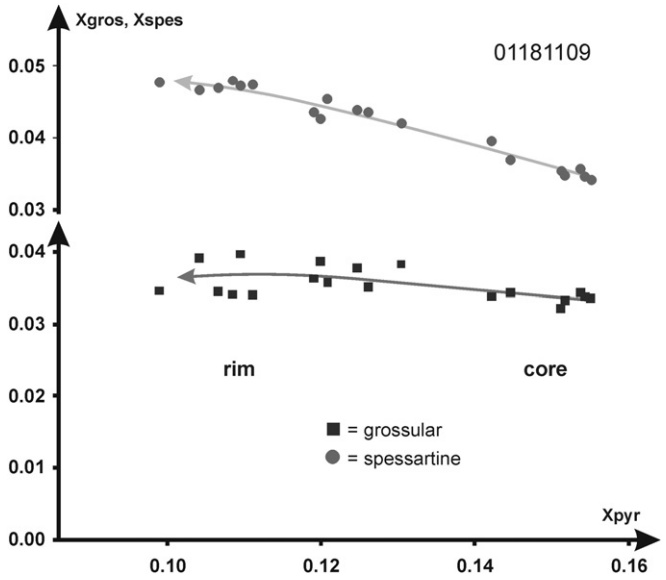

Fig. 5. Analyses of garnet in altered granite 01181109 in terms of molar fractions of grossular (+andradite) and spessartine versus that of pyrope. The solid lines show the chemical trends from core to garnet rim compositions.

the Tschermak's substitution. Correspondingly, somewhat more than 1 wt% and 0.5 wt% of FeO and MgO, respectively, were often analyzed to occur in potassic white mica. Typically, muscovite with the higher Si contents within the above given range contains some Ti whereas in the low Si muscovite no Ti was detected. In addition, Ti was analyzed in muscovite when the analytical spot was located rather in the center of larger grains. Muscovite, formed from Ti-free feldspars, cannot introduce Ti, whereas muscovite crystallizing from Ti-bearing melt can incorporate this element. For this reason (see Massonne et al., 2010), we suggest that Ti-bearing muscovite with Si contents around 3.11 pfu is a late-magmatic phase that grew further, replacing feldspar at a post-magmatic stage, with lower Si contents around 3.07 pfu. Muscovite in sample 01181109 contains up to 6 mol

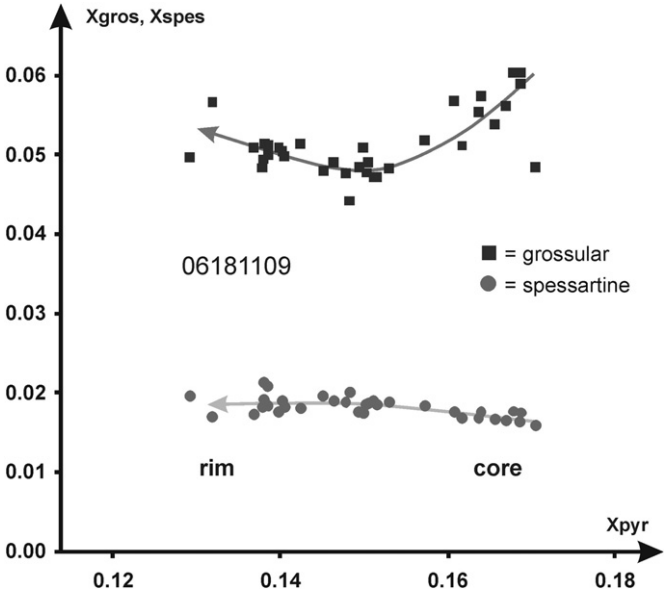

Fig. 6. Analyses of garnet in metapelite 06181109 in terms of molar fractions of grossular (+andradite) and spessartine versus that of pyrope. The solid lines show the chemical trends from core to garnet rim compositions.

% paragonite component and some Ba (Table 2). The composition of biotite in the garnet-bearing gneiss seems to be rather homogeneous as the observed variety of compositional data for this mineral can be explained by the analytical error. Biotite contains around 2.70 Si pfu. Contents of TiO_2 are high, scattering around 3.5 wt%. In addition, biotite contains some Na, Ba, and F (see Table 2).

Plagioclase in the altered granite is albite whereas plagioclase in the biotite gneiss is andesine with 30–35 mol% anorthite component. K-feldspar in the altered granite contains a few mol% of albite component only. Ilmenite analyses yielded some Mn and Mg. In addition, some hematite component in this phase resulted from the calculation of the structural formula of ilmenite (Table 2).

5.2. *P–T* path

As we wanted to gain access to the metamorphic evolution, we considered the *P–T* pseudosections of sample 06181109 first. The composition of this sample (Table 1) is that of a pelitic rock. Therefore, the calculation of the *P–T* pseudosection resulted in mineral assemblages typical for metapelites such as those with staurolite at temperatures between 530 and 650 °C and pressures between 2 and 8 kbar (Fig. 7). Kyanite or sillimanite appear at higher temperatures. Cordierite occurs at pressures below 5.5 kbar and at temperatures above 490 °C (1 kbar). Biotite is present in almost the entire *P–T* range of the pseudosection of Fig. 7 except in a range of the highest temperatures and lowest pressures. On the contrary, potassic white mica solely appears at temperatures below 500 °C and again at higher temperatures, but only above 7 kbar. Chlorite is a common phase at temperatures below 600 °C. The solidus curve for silicate melt reaches temperatures as low as 670 °C at the highest pressures of the *P–T* pseudosection for sample 06181109.

In contrast to the metapelite, the *P–T* pseudosection for the granitic composition (see Table 1) is simpler in terms of the number of assemblages appearing in the *P–T* frame of 1–9 kbar and 450–750 °C (Fig. 8). K-feldspar is omnipresent within this *P–T* frame. Plagioclase is a common phase in the calculated mineral assemblages except at high pressures and low temperatures where jadeite-rich clinopyroxene appears instead. Compared to the *P–T* pseudosection of the studied metapelite, the *P–T* ranges for biotite and potassic white mica are smaller and larger, respectively, in the pseudosection for the granitic composition. Although only 1 wt % H_2O was considered for the granitic composition, the calculated *P–T* position of the solidus curve is located at significantly lower temperatures compared to that in the pseudosection for the pelitic composition with even 3.5 wt% H_2O.

Garnet appears in both pseudosections of Figs. 7 and 8 over a wide *P–T* range and is chemically inhomogeneous in the studied rocks. For these reasons, the *P–T* pseudosections were contoured with isopleths for the molar fractions of garnet components (Figs. 9 and 10). Typically, the molar fraction of the pyrope component (=XMg) increases with rising pressure and temperature reaching maximum values of somewhat above and below 0.20 for the metapelite and the altered granite, respectively, at the highest temperatures and pressures of the *P–T* pseudosections. This trend is opposed in the analyzed garnets from core to rim in both samples (see Figs. 4–6). Consequently, when deriving a *P–T* path from the observed garnet compositions and the *P–T* pseudosections contoured by molar fractions of garnet components, only a retrograde path (or cooling path for the igneous rock) can result.

On the basis of the aforementioned core composition of garnet in sample 06181109 a *P–T* condition of 6.7 kbar and 670 °C can be deduced (Fig. 11) using the correspondingly contoured *P–T* pseudosection. The garnet rim composition yields conditions of 4.5 kbar and 600 °C. However, the *P–T* path is not characterized by a straight line in a *P–T* diagram between the given conditions. Using the

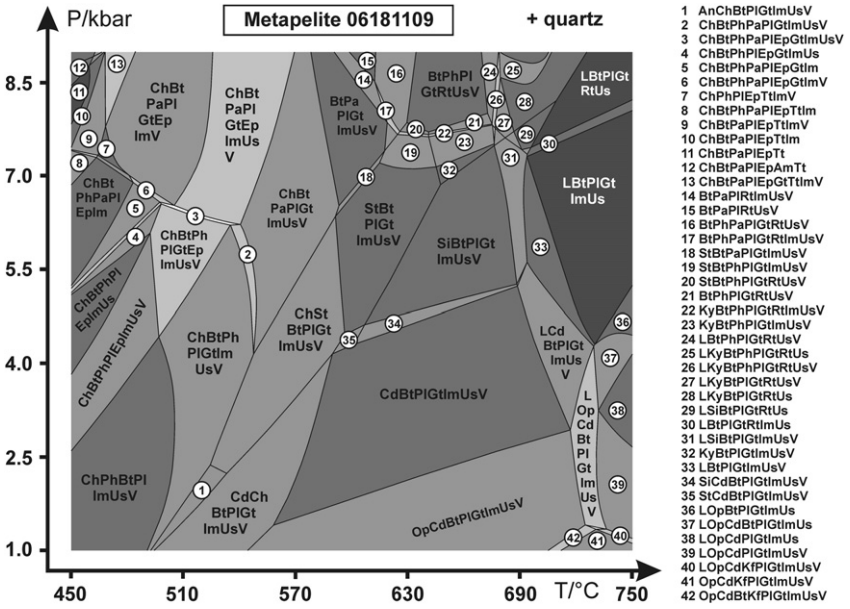

Fig. 7. *P–T* pseudosection calculated for the simplified composition of metapelite 06181109 (Table 1) with the computer software package PERPLE_X (see text). Abbreviations: Am = amphibole, An = andalusite, Bt = biotite, Cd = cordierite, Ch = chlorite, Ep = epidote, Gt = garnet, Im = ilmenite, Kf = alkalifeldspar, Ky = kyanite, L = melt, Op = orthopyroxene, Pa = paragonite, Ph = phengite–muscovite, Pl = plagioclase, Q = quartz, Rt = rutile, Si = sillimanite, St = staurolite, Tt = titanite, Us = ulvöspinel–magnetite, V = H_2O vapor.

chemical evolution of garnet from core to rim as shown in Fig. 6, the path would first possess a steep d*P*/d*T*-slope leading to *P–T* conditions of about 5 kbar and 650 °C and subsequently flatten out (see Fig. 11) to consider the decrease in Ca from core to intermediate garnet zone and the following increase towards the garnet rim. The absence of potassic white mica, cordierite, staurolite, and former melt in the metapelite 06181109 is compatible with this path. It is assumed that the *P–T* path continues more or less linearly to surface conditions, but staurolite formation below 600 °C did not take place probably due to the absence of a hydrous fluid to form staurolite from garnet in a complex reaction. The derived temperature regime for the (solid) *P–T* path of Fig. 11 is also constrained by Fe^{2+}–Mg exchange geothermometry (see below) applied to the pair biotite–garnet. Using the garnet core and biotite compositions given in Table 2 for metapelite 06181109, temperatures of 631 °C and 645 °C at 4 and 8 kbar, respectively, result. For the garnet rim composition (Table 2) these temperatures are 577 °C and 590 °C. The use of the Si content in biotite (~2.70 pfu) with the TiBio(HP) model (see the Si isopleths in Fig. 10) points to pressures either above 8 kbar or below 3.5 kbar at the here relevant temperatures. For the derived *P–T* path these contents should be between 2.59 and 2.64 Si per formula unit. As the quality of the

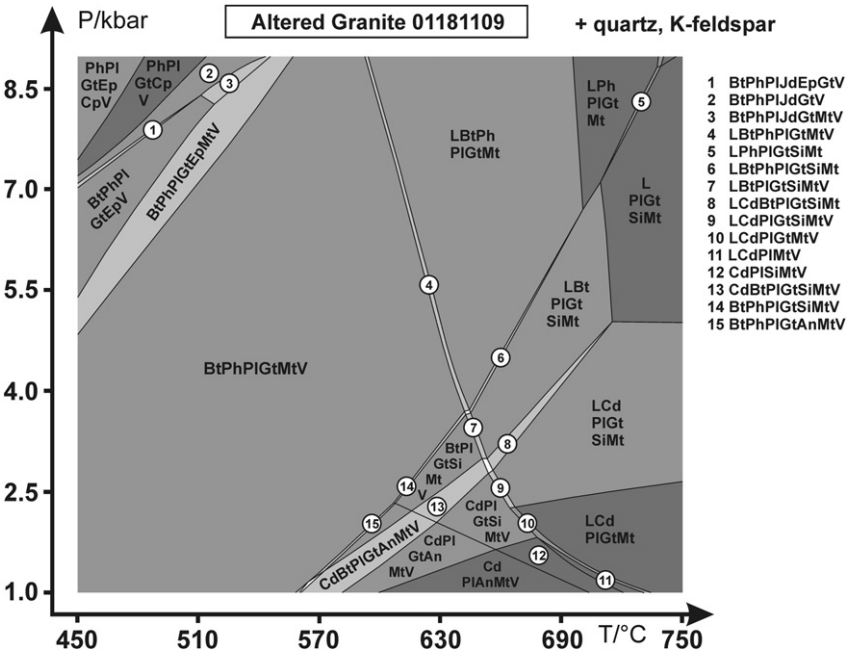

Fig. 8. *P–T* pseudosection calculated for the simplified composition of altered granite 01181109 (Table 1) with the computer software package PERPLE_X (see text). Abbreviations as in Fig. 7 and Mt = magnetite.

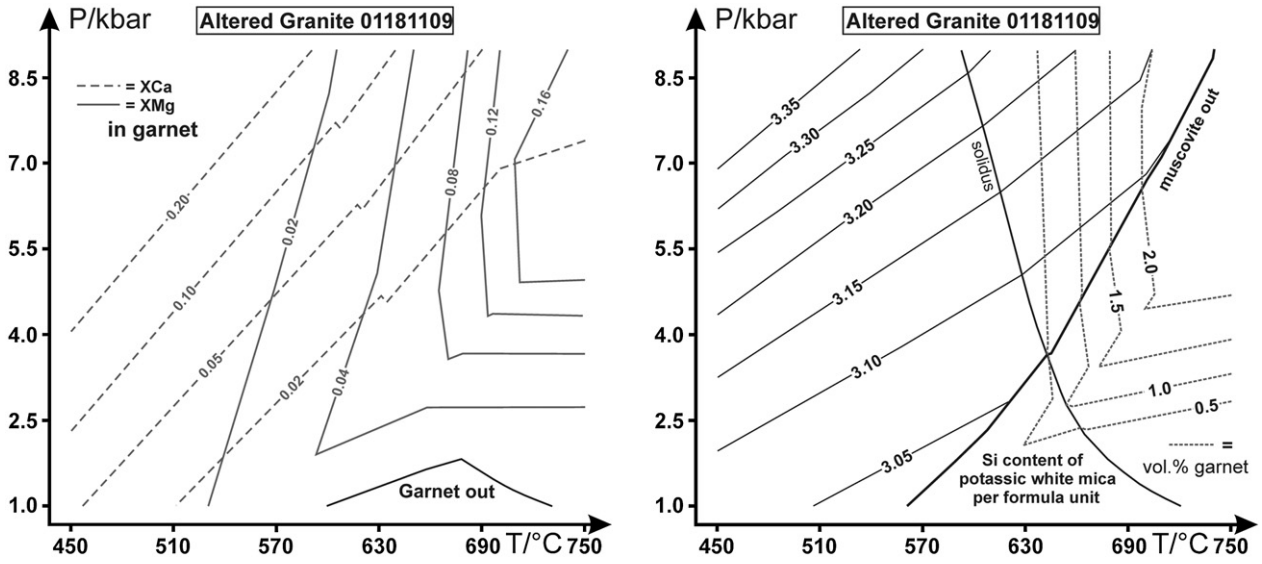

Fig. 9. *P–T* pseudosection of Fig. 8 contoured by isopleths for molar fractions of Ca and Mg in garnet (left hand side), Si contents pfu in potassic white mica and vol.% of garnet in the rock (right hand side).

thermodynamic model for biotite is significantly worse compared to that for potassic white mica (model Pheng(HP)), which is, in contrast to the biotite model, based on several experimental studies (e.g. Massonne and Szpurka, 1997), we did not take the geobarometric result of the Si content in biotite into account.

In the same way as for metapelite 06181109, the *P–T* conditions were deduced for garnet in the altered granite using the contoured *P–T* diagram of Fig. 9. The result is a magmatic cooling path shown in Fig. 11. This path starts at 7.95 kbar and 715 °C and ends at 7.5 kbar and 690 °C. Igneous muscovite with Si contents around 3.11 pfu (see above) crystallized latter, very likely at *P–T* conditions somewhat above 6 kbar and 650 °C (see Si isopleths for potassic white mica in Fig. 9). These conditions are compatible with the *P–T* path derived from the compositions of garnet in the metapelite.

6. Age dating

6.1. Analytical method

Relatively large (occasionally somewhat more than 100 μm in diameter) but marginally corroded monazite occurs in metapelite 06181109. Some of these monazite grains were dated with the aforementioned CAMECA SX100 EMP. Measurement conditions were 150 nA and 20 kV for beam current and acceleration voltage, respectively, using a focussed beam. For each full analysis of monazite, the most common rare-earth elements (REEs) and Pb, U, Th, P, Ca, Si, and Y were measured using the following emission lines, standards and counting times on peak and background: Si Kα, wollastonite, 200 s; P Kα, La-phosphate, 20 s; S Kα, barite, 50 s; Ca Kα, wollastonite, 20 s; Y Lα, Y-phosphate, 280 s; La Lα, La-phosphate, 20 s; Ce Lα, Ce-phosphate, 20 s; Pr Lβ, Pr-phosphate, 160 s; Nd Lβ, Nd-phosphate, 100 s; Sm Lβ, Sm-phosphate, 300 s; Gd Lβ, Gd-phosphate, 160 s; Dy Lβ, Dy-phosphate, 160 s; Pb Mα, PbTe, 500 s; Th Mα, Thorite; 140 s; U Mβ, U metal, 250 s. Oxygen was calculated by stoichiometry. Uranium and Th were measured with a normal-sized PET spectrometer crystal whereas Pb was analyzed with a large PET crystal. Similar to Scherrer et al. (2000), a (small) correction of the U Mβ peak was applied because of the contribution from the Th Mγ line. Furthermore, a correction of the Pb Mα radiation for interferences with Th and Y lines was achieved (see Jercinovic and Williams, 2005; Pyle et al., 2005). All REEs were measured with LIF spectrometer crystals. For the background measurements of the REEs, we followed the recommendations by Reed and Buckley (1998).

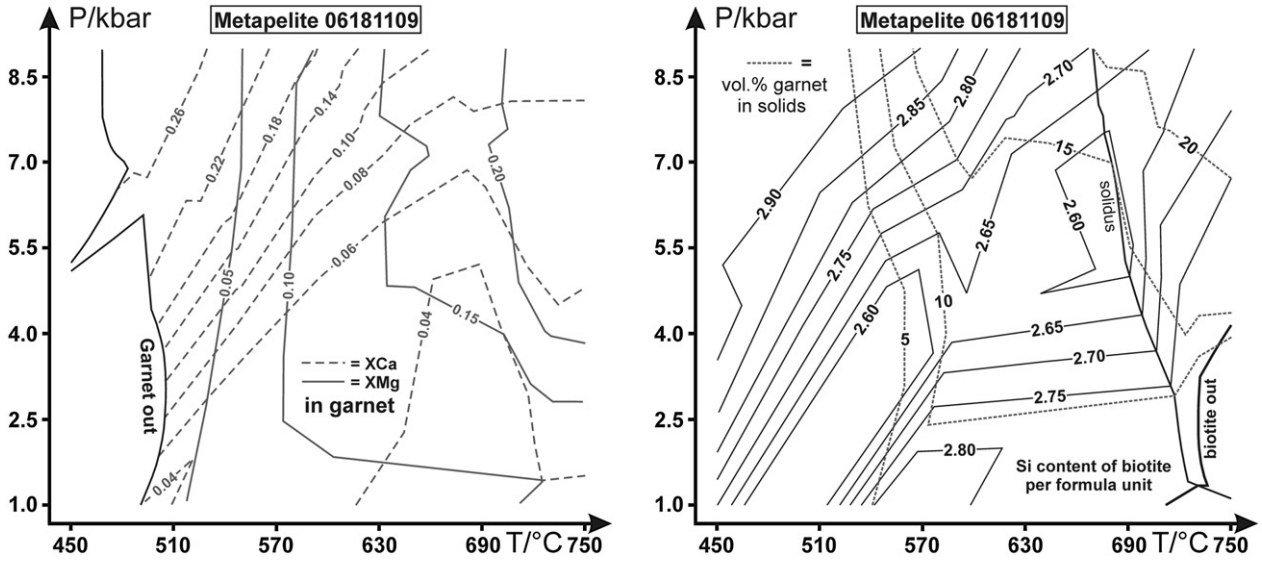

Fig. 10. *P–T* pseudosection of Fig. 7 contoured by isopleths for molar fractions of Ca and Mg in garnet (left hand side), Si contents pfu in biotite and vol.% of garnet in the rock (right hand side).

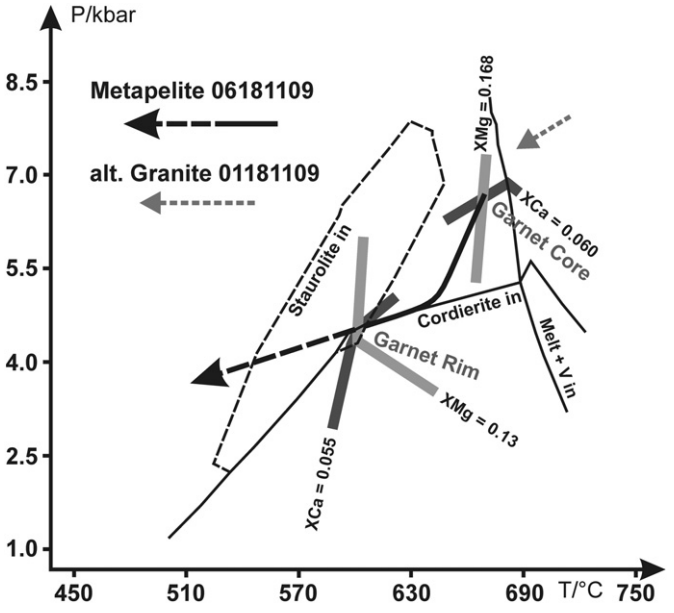

Fig. 11. *P–T* path for the Cinco Cerros basement reconstructed on the basis of the garnet zonation in metapelite 06181109. The relevant garnet compositions and *P–T* boundaries of specific phases are given. The grey dashed *P–T* path shows the crystallization conditions during growth of garnet in the altered granite 01181109.

We have tested the above analytical conditions against Early Ordovician monazite from Brazil (see Massonne et al., 2007) and Late Tertiary monazite from the Himalaya (see Liu et al., 2011) which were also dated with a SHRIMP and a TIMS, respectively. As we were able to reproduce the ages determined by mass spectrometry, we are confident that the here presented ages are precise within the given errors of the single analysis (Table 3). These errors were calculated with the MINCALC-V5 software by Bernhardt (2007).

6.2. Resulting ages

Altogether 16 monazite U–Th–Pb ages were obtained after selection of analyses. Those were discarded which are characterized, for instance, by too high Si contents or low totals typical for analyses of spots close to the margin of corroded monazite. The remaining monazite analyses show variable contents of elements specifically Th, U and REE (Table 3, Fig. 12). These analyses could be grouped on the basis of ages and chemical composition. The oldest group I with an age cluster at 2073 ± 11.4 (1σ) Ma is characterized by relatively high Th (average: 2.53 wt% ThO_2), moderate U (average: 0.25 wt% UO_2) and low Y (average: 0.10 wt% Y_2O_3) contents. The average contents of CaO and Gd_2O_3 (not shown in Fig. 12) are 0.56 and 0.80 wt%, respectively. A further group II is chemically similar to I (average: 2.38 wt% ThO_2, 0.64 wt% UO_2, 0.10 wt% Y_2O_3, 1.19 wt% CaO, 0.85 wt% Gd_2O_3) but is significantly younger (1913 ± 11.0 Ma) than age group I. The youngest group III (1805 ± 20.8 Ma; 0.01 wt% ThO_2, 0.74 wt% UO_2, 0.33 wt% Y_2O_3, 0.58 wt% CaO, 1.86 wt% Gd_2O_3) is both clearly younger than II and chemically different to I and II. The latter statement also concerns the La and Nd concentrations in monazite of group III which are lower and higher, respectively, compared to those of groups I and II (see Fig. 12). Thus, the REE patterns of monazites of group III must be significantly flatter (concentrations of heavy REE and also Y are relatively high in group III) than those of the other monazites. This is interpreted by the release of Y and heavy REE from garnet, in which such elements are usually enriched, and their introduction in newly formed monazite in the absence of coexisting (in a thermodynamic sense) garnet.

Table 3
EMP analyses of monazite in metapelite 06181109. The calculated structural formula of this mineral is based on 4 oxygens. For age determination see text.

Anal.-no.	2203-2	2203-15	2203-18
SiO_2 in wt%	0.29	0.25	0.26
P_2O_5	29.37	29.38	29.50
SO_3	0.00	0.01	0.03
CaO	0.38	0.66	0.57
Y_2O_3	0.43	0.17	0.00
La_2O_3	11.03	13.37	14.84
Ce_2O_3	30.39	31.55	32.02
Pr_2O_3	3.84	3.49	3.42
Nd_2O_3	16.38	13.87	13.50
Sm_2O_3	3.53	2.47	2.06
Gd_2O_3	1.77	1.17	0.27
Dy_2O_3	0.00	0.00	0.00
PbO	0.224	0.389	0.324
ThO_2	0.00	1.59	2.61
UO_2	0.77	0.84	0.28
Total	98.84	99.40	99.66
Si	0.0114	0.0100	0.0103
P	0.9884	0.9867	0.9880
S	0.0001	0.0004	0.0008
Ca	0.0163	0.0282	0.0241
Y	0.0092	0.0036	0.0000
La	0.1618	0.1957	0.2165
Ce	0.4423	0.4583	0.4637
Pr	0.0556	0.0505	0.0493
Nd	0.2325	0.1966	0.1907
Sm	0.0483	0.0338	0.0281
Gd	0.0233	0.0154	0.0035
Dy	0.0000	0.0000	0.0000
Pb	0.00240	0.00415	0.00345
Th	0.0000	0.0144	0.0235
U	0.0068	0.0074	0.0024
Cation sum	2.0077	2.0087	2.0043
Age in Ma	1814	1896	2056
1σ in Ma	33.4	22.1	25.9

7. Discussion

The above derived *P–T* paths for a metapelite and an altered granite allow us to gain new insights into the evolution of the RPC crust in the region of the Cinco Cerros area. The zonation of garnet in the granite points to a pressure release from 8 to 7.5 kbar at decreasing temperatures (Fig. 11). This can be explained by crystallization of garnet in an uprising granitic melt at temperatures around 700 °C before the formed crystal mush settled between the gneisses of the Cinco Cerros area. There, it finally crystallized completely at the conditions of the surrounding rocks. About 6.5% melt (PERPLE_X calculation result not shown in Figs. 8 and 9) is still present in the granitic crystal mush at 670 °C (after crystallization of the garnet) and 7 kbar compatible with the aforementioned view of the emplacement of the granite. Among the adjacent rocks of the granite is the studied unmelted metapelite. The zonation of garnet in this rock suggests an exhumation by 7 km from crustal levels of ca. 25 km (6.7 kbar) at decreasing temperatures from 670 to 600 °C (Fig. 11). However, in contrast to growing garnet in a granitic melt, the decreasing temperatures resulted in a resorption of garnet (see Fig. 10). The PERPLE_X calculations yielded a diminishment of the garnet volume from 14.8 to 12.9 vol.% along the derived exhumation path. Nevertheless, a garnet rim with a poorly defined thickness in the range of 100 μm is always discernible in the chemical zonation patterns (see Fig. 4). This rim points to equilibration with surrounding minerals. Thus, there is no growth zonation in garnet of the studied metapelite but a zonation probably due to a late-stage cation diffusion. An alternative view was recently uttered

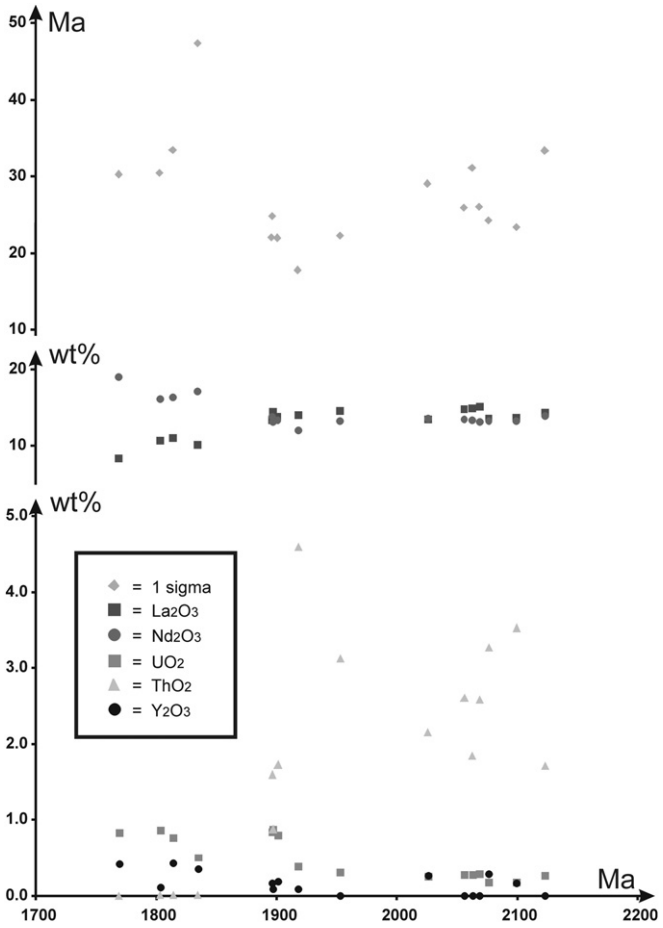

Fig. 12. Contents of specific elements (given as oxides) in monazite as well as uncertainties of the single U–Th–Pb age determinations on this mineral versus the determined age.

by Martin et al. (2011) who suggested that re-equilibration of such garnets could also be due to a combination of dissolution and re-precipitation. However, if we relate our ages obtained on monazite with relatively low Y and Gd contents (groups I and II, see above) to the coexistence with garnet, then there is a period of time of more than 150 million years (starting at 2070 Ma) meanwhile cation diffusion was acting at temperatures between 600 °C and 670 °C. This period of time was probably sufficient to produce such a relatively narrow late equilibration zone at the garnet rims. The shape of the *P–T* path in Fig. 11 is more problematic, because of an intermediate garnet composition, between core and rim, that could have been also somewhat altered by the mentioned cation diffusion. However, Ca contents in intermediate garnet compositions of the studied metapelite (see Fig. 6) are lowest. If these compositions were influenced by cation diffusion, the Ca would have been once even lower. Thus, the shape of the *P–T* paths could have been even more crooked than shown in Fig. 11, i.e. a nearly isothermal exhumation was followed by a nearly isobaric cooling down to 600 °C at 4.5–5 kbar. After this stage, the continuation of a slow cooling process is likely, so that the Cinco Cerros area was probably close to the surface in Mesoproterozoic to early Neoproterozoic times. For the early metamorphic path (not shown in Fig. 11) an assumption with a similar high probability cannot be made. Nevertheless, it is conceivable that the *P–T* conditions of 6.7 kbar and 670 °C, recorded by the core of the metapelitic garnet, were reached by a prograde evolution especially by (nearly isobaric?) heating due to the emplacement of adjacent large granitoid bodies including smaller bodies such as the granitic layer from which sample 01181109 was taken. The pressure conditions around 6 kbar, which were derived by Delpino and Dristas (2008) for nearby calc–silicate rocks, are compatible with our estimates. However, the temperatures of 750–800 °C for the early metamorphism given by these authors are higher than those deduced here. We think that metamorphic temperatures of 750 °C and more would have resulted in a higher degree of melting than observed in the Cinco Cerros area. However, we cannot exclude that the basement area studied by Delpino and Dristas (2008), although located only 9 km southeast of the Cinco Cerros area, has experienced a higher metamorphic grade.

After the derivation of the *P–T–t* path for the Cinco Cerros area the question arises which geodynamic scenario could be responsible for this path and the related monazite ages (see Section 6.2). Additional information, such as that of the geochemical character and abundance of the widespread and partially deformed granitoid bodies, should be considered for this scenario as well. In Fig. 13, we present such as geodynamic scenario in a two-dimensional sketch. If the U–Pb ages of zircon from (meta)granitoids are related to the time of magma crystallization, granitic melts intruded the presently exposed crustal level mainly in the time interval 2.1–2.2 Ga. If we consider the entire RPC, the oldest ages are around 2.25 Ga (Hartmann et al., 2002). Ages younger than 2.1 Ga for zircon in (meta)granitoids are rare. With this in mind, we propose a collisional scenario, that started ca. 2.2 Ga or earlier and is characterized by the submersion of oceanic crust (probably somewhat thicker than normal, present-day oceanic crust, but not as thick as old Archean oceanic crust – see, e.g., Rollinson, 2010) beneath a cratonic area (for which a thickness of 40 km was assumed in Fig. 13) which could be called proto-RPC. Instead of a subduction process invoked by previous authors addressing the formation of the RPC (see, e.g. Cingolani, 2011), we suggest an underthrust process because it is highly questionable whether eclogitization of oceanic crust commonly occurred already in Paleoproterozoic times when geotherms were significantly higher than today. Without eclogitization, subduction of oceanic crust should not occur. The very rare examples of eclogite in Paleoproterozoic (e.g. Boniface et al., 2012) and older crust (e.g. Shchipansky et al., 2012) can also be explained by crustal thickening as suggested in our model of Fig. 13. However, subduction-related eclogites are definitely known from collisional belts younger than 1 Ga (see Massonne, 2004; Stern, 2008). At least eclogites do not occur in the RPC. Even if the basic oceanic crust was not subducted but only underthrust, melts could have been generated in this crust because such an underthrust process will result in a heating of the submersed basic material. Acidic to intermediate melts should be formed by fluid-absent partial melting of oceanic crust at 12–16 kbar characterized by a solidus at ca. 900 °C (see, e.g. summary of experimental works by Moyen and Stevens, 2006). Garnet-rich restites, formed by this melting process, may delaminate (see, e.g. Rudnick, 1995) to be one factor in the reduction of the thickened collisional crust to present-day values close to a thickness of 40 km (Kostadinoff, 1995; Del Cogliano, 2006). The Sm–Nd model ages of ca. 2.4–2.7 Ga reported for the granitoids in the RPC (Hartmann et al., 2002; Pankhurst et al., 2003), confirmed by recent model ages on the basis of Hf isotopes (Cingolani et al., 2010), are explained here by inheritance from the underthrust oceanic crust, which would mean that this crust had formed from partially molten mantle in late Archean to early Paleoproterozoic times.

As the melts, ascending from the underthrust oceanic crust, intruded mid-crustal levels in regard of the thickened crust, material, such as the studied metapelites, were heated close to 700 °C and partially migmatized. This happened for the Cinco Cerros area about 2.07 Ga ago according to the cluster of the oldest

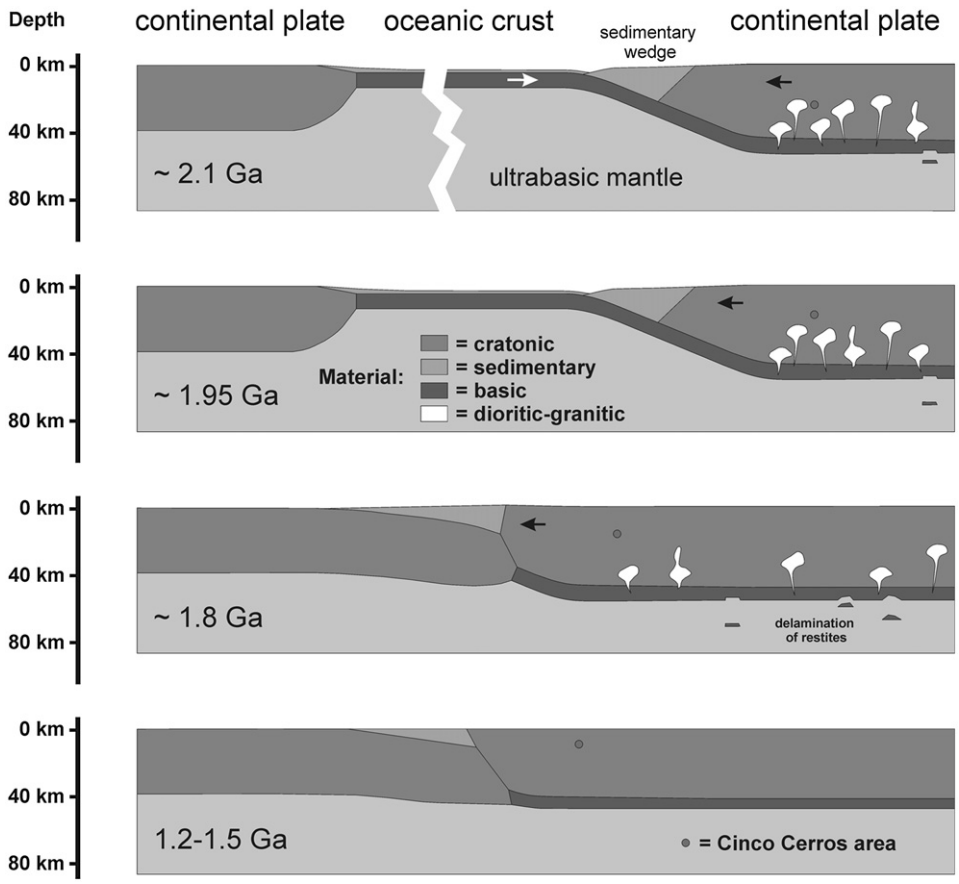

Fig. 13. Sketch of a collisional scenario in Paleoproterozoic times to explain the evolution of the Cinco Cerros basement, shown by the dark grey dot.

monazites analyzed. From this time on, the Cinco Cerros crustal level cooled slowly down although melts continued to ascend from the base of the thickened crust. However, these melts intruded for the following $\geq$0.2 Ga lower crustal levels so that the crust remained nearly as thick as before also because of continuous erosion at the surface. This erosion led to a slow exhumation of the Cinco Cerros area, so that this area reached a level of 15–18 km depth at 1.91 Ga. Finally, the collisional process ended perhaps soon after and the thickened crust approached from then on normal cratonic crustal thicknesses in the following 0.5–1 Ga.

A thermotectonic and probably fluid-related event is hypothesized for the youngest monazite age at 1.81 Ga. Around Tandil, ca. 70 km northwest of the Cinco Cerros area (Fig. 1), and further northwestwards, suites of calc–alkaline and tholeiitic dikes were recognized which had formed in the time interval from 2.0 to 1.6 Ga according to Iacumin et al. (2001) and Texeira et al. (2002). The younger suite of tholeiitic dikes is believed by these authors to constrain the time of crustal extension at the Paleoproterozoic boundary of the RPC. The 1.81 Ma age obtained from monazite is in the range of ages for these dikes. In addition, Bossi et al. (1993) gave an age of 1.86 $\pm$ 0.12 Ga for such undeformed dikes from the RPC of Uruguay. Somewhat younger ages around 1.74 Ga were reported by Texeira et al. (1999). Furthermore, weak ductile deformation up to the formation of real mylonites occurred in the Cinco Cerros area as the last event. Such mylonites are common in the Tandilia belt with the classical area of the Azul megashear zone (Frisicale et al., 2005 and references therein). Unfortunately, the time of formation of these mylonites is not well constrained yet. Nevertheless, we speculate that the youngest monazite suggest the time of mylonite formation around 1.81 Ga also because the relatively young tholeiitic dikes are undeformed. This monazite formed from garnet (see above) which (partially) decomposed below 500 °C (Fig. 10). Following the deduced exhumation path of the studied metapelite (Fig. 11), pressures not much lower than 4 kbar are expected for the ductile deformation event leading to mylonites. However, a pressure range of 6–9 kbar was estimated by Frisicale et al. (2005, 2010, 2012) for the formation of mylonites from different localities of the aforementioned Azul megashear zone.

As the rock types, exemplary studied in the Cinco Cerros area, are widespread in the RPC, we believe that the above scenario could be applicable to the RPC, in general. Unfortunately, there are only a very few works that have also estimated the peak pressure of metamorphic rocks from the RPC (see Section 2.2). These estimates range between 5 and 10 kbar confirming our view that the original medium to lower crustal levels of the RPC are commonly exposed today. The exposed rocks were relatively hot (up to 700 °C) once. Our geodynamic model explains the wide distribution of hot, medium crustal rocks, penetrated by abundant dioritic to granitic bodies. Moreover, this model is compatible with the slow cooling and exhumation of the RPC crust by erosional processes, as recorded by the kind of garnet zonation and the analyzed monazite ages. Previous models (Teruggi et al., 1988; Ramos et al., 1990; Hartmann et al., 2002, 2003; Pankhurst et al., 2003; Delpino and Dristas, 2008; Cingolani, 2011) considered only the accretion of major terranes in Paleoproterozoic times resulting in the assembly of a proto-South American plate. This accretion was mainly explained by subduction of oceanic crust between these terranes also causing the widespread intrusions of (meta)plutonic rocks of intermediate to acidic composition which formed magmatic arcs (e.g. Pankhurst et al., 2003; Rapela et al., 2007). The authors of these models might have

had in mind the Cenozoic evolution of Earth during which magmatic arcs formed indeed by subducted oceanic crust and, after complete subduction, continent–continent collision occurred. However, independent evidence of subduction processes by high pressure rocks, as common for Cenozoic continent–continent collisional belts, are lacking in the RPC. In addition, the chemical composition of the magmas that had intruded the RPC crust is different from those of Cenozoic magmatic arcs. By contrast, our model also explains the intensive and geographically widespread occurrence of such magmatic rocks. Especially the latter characteristic is not typical for Cenozoic magmatic arcs. A much flatter subduction in Paleoproterozoic times than today could be an argument for the geographically widespread occurrence of the 2.0–2.2 Ga old magmatic rocks of the RPC. According to our model a subduction of oceanic crust is not necessary but underthrusting of this crust without eclogitization.

8. Conclusions

Our petrological study resulted in a well-corroborated metamorphic *P–T–t* path starting at conditions of 6.7 kbar and 670 °C. The final metamorphic conditions were 4.5 kbar and 600 °C. This *P–T* evolution and the timing, elucidated by EMP geochronology on monazite, as well as the overall geological situation of the exposed RPC in the Tandilia belt can be well explained by a long-lasting collision of oceanic crust with the proto-RPC. The oceanic crust was thrust under this craton to generate intermediate to acidic partial melts that penetrated mid-crustal levels of the thickened, collisional crust. The penetration by large melt volumes caused the heating of the middle crust close to 700 °C causing widespread anatexis in the currently exposed crustal level at 2.07 Ga. This crustal level was very slowly exhumed by ca. 7 km (difference between the aforementioned pressures of 6.7 and 4.5 kbar) within 0.15 Ga. In this time interval the temperature dropped by ca. 70 °C. Afterwards this exhumation process slowed down so that finally the Cinco Cerros area and other exposed regions of the RPC were close to the surface not before Mesoproterozoic to Neoproterozoic times. Also the underthrusting of oceanic crust might have continued after 1.91 Ga, but when it finally stopped remains unclear.

Acknowledgements

This research was financially supported by the Alexander von Humboldt Foundation within the co-operation project: Projekt/V-Fokoop_ARG/1005980. The electron microprobe work at Universität Stuttgart was supported by Thomas Theye. We also thank two anonymous reviewers for their constructive comments.

References

Basei, M.A.S., Peel, E., Sánchez Bettucci, L., Preciozzi, F., Nutman, A.P., 2011. The basement of the Punta del Este terrane (Uruguay): an African Mesoproterozoic fragment at the eastern border of the South American Río de La Plata Craton. International Journal of Earth Sciences 100, 289–304.

Bernhardt, H.-J., 2007. MINCALC-V5, a software tool for mineral analyses data processing. Acta Microscopica 16 (Suppl. 2), 43–44.

Bohlen, S.R., Mezger, K., 1989. Origin of granulite terranes and the formation of the lowermost continental crust. Science 244, 326–329.

Boniface, N., Schenk, V., Appel, P., 2012. Paleoproterozoic eclogites of MORB-type chemistry and three Proterozoic orogenic cycles in the Ubendian Belt (Tanzania): evidence from monazite and zircon geochronology, and geochemistry. Precambrian Research 192–195, 16–33.

Bossi, J., Cingolani, C.A., 2009. Extension and general evolution of the Río de la Plata Craton. In: Gaucher, C., Sial, A.N., Halverson, G.P., Frimmel, H.E. (Eds.), Neoproterozoic-Cambrian Tectonics, Global Change and Evolution: A Focus on Southwestern Gondwana. Developments in Precambrian Geology, vol. 16, pp. 73–85.

Bossi, J., Campal, N., Civetta, L., Demarchi, G., Girardi, V.A.V., Mazzucchelli, M., Negrini, L., Rivalenti, G., Fragoso Cesar, A.R.S., Sinigoi, S., Teixeira, W., Picirillo, E.M., Molesini, M., 1993. Early Proterozoic dike swarms from western Uruguay: geochemistry, Sr–Nd isotopes and petrogenesis. Chemical Geology 106, 263–277.

Braga, R., Massonne, H.-J., 2012. H_2O content of deep-seated orogenic continental crust: the Ulten Zone, Italian Alps. International Geology Review 54, 633–641.

Cingolani, C.A., 2011. The Tandilia system of Argentina as a southern extension of the Río de la Plata Craton: an overview. International Journal of Earth Sciences 100, 221–242.

Cingolani, C.A., Dalla Salda, L., 2000. Buenos Aires cratonic region. In: Cordani, U.G., Milani, E.J., Filho, A.T., Campos, D.A. (Eds.), Tectonic Evolution of South America. 31st International Geological Congress, Rio de Janeiro, Brazil, pp. 139–147.

Cingolani, C.A., Hartmann, L.A., Santos, J.O., McNaughton, N.J., 2002. U–Pb SHRIMP dating of the zircons from the Buenos Aires Complex of the Tandilia Belt, Río de la Plata Craton, Argentina. In: XV Congreso Geológico Argentino, El Calafate, Argentina, Actas, vol. 1, pp. 149–154.

Cingolani, C.A., Santos, J.O.S., McNaughton, N.J., Hartmann, L.A., 2005. Geocronología U–Pb SHRIMP sobre circones del granitoide Montecristo, Tandil, provincia de Buenos Aires, Argentina. In: XVI Congreso Geológico Argentino, Actas, vol. 1, pp. 299–302.

Cingolani, C.A., Santos, J.O.S., Griffin, W., 2010. New insights of the Paleoproterozoic basement of Tandilia belt, Río de la Plata Craton, Argentina: first Hf isotope studies on zircon crystals. Bollettino di Geofisica Teorica ed Applicata 51 (Suppl), 21–24.

Connolly, J.A.D., 1990. Multivariable phase diagrams; an algorithm based on generalized thermodynamics. American Journal of Science 290, 666–718.

Connolly, J.A.D., 2005. Computation of phase equilibria by linear programming: a tool for geodynamic modeling and its application to subduction zone decarbonation. Earth and Planetary Science Letters 236, 524–541.

Cordani, U.G., D'Agrella-Filho, M.S., Brito-Neves, B.B., Trindade, R.I.F., 2003. Tearing up Rodinia: the Neoproterozoic palaeogeography of South American cratonic fragments. Terra Nova 15, 350–359.

Cortelezzi, C.R., Ribot, A.M., De Barrio, R.E., 1999. Los gneises piroxénicos del basamento precámbrico de las Sierras de Balcarce, Tandilia, Argentina. In: XIV Congreso Geológico Argentino, Salta, Actas, vol. 2, pp. 90–91.

Dalla Salda, L., Iñiguez, A.M., 1979. La Tinta, Precámbrico y Paleozoico de Buenos Aires. In: VII Congreso Geológico Argentino, Actas, vol. 1, pp. 539–550.

Dalla Salda, L.H., Franzese, J.R., Posadas, V.G., 1992. The 1800 Ma Mylonite–Anatectic granitoid association in Tandilia, Argentina. In: Mason, R. (Ed.), 1992. Basement Tectonics, vol. 7. Kluwer Academic Publishers, pp. 161–174.

Dalla Salda, L., De Barrio, R.E., Echeveste, H.J., Fernández, R.R., 2005. El basamento de las Sierras de Tandilia. In: De Barrio, R.E., Etcheverry, R.O., Caballé, M.F., Llambías, E. (Eds.), Geología y Recursos Minerales de la Provincia de Buenos Aires. Relatorio del XVI Congreso Geológico Argentino, Actas, vol. 4, pp. 31–50.

Dalla Salda, L.H., Spalletti, L.A., Poiré, D.G., De Barrio, R., Echeveste, H., Benialgo, A., 2006. Tandilia. Temas de Geología Argentina 1. Serie Correlación Geológica 21, 17–46.

Del Cogliano, D., 2006. Modelado del Geoide con GPS y Gravimetría. Caracterización de la Estructura Geológica de Tandil. Unpubl.. Ph.D. thesis, Facultad de Ciencias Exactas, Ingeniería y Agrimensura, Universidad Nacional de Rosario, Rosario, Argentina, p. 103.

Delpino, S.H., 2000. Evolución metamórfica del sector nororiental del basamento de Tandilia, Argentina: metamorfismo en facies granulita y anatexis cortical. Unpubl.. Ph.D. thesis, Universidad Nacional del Sur, Bahía Blanca, Argentina, p. 180.

Delpino, S.H., Dristas, J.A., 1999. Estudio petrográfico-microestructural sobre las rocas metamórficas félsicas e intermedias del sector nororiental del basamento de Tandilia. Revista de la Asociación Geológica Argentina 54, 152–172.

Delpino, S.H., Dristas, J.A., 2008. Dolomitic marbles and associated calc-silicates, Tandilia belt, Argentina: geothermobarometry, metamorphic evolution, and *P–T* path. Journal of South American Earth Sciences 25, 501–525.

Di Paola, E.C., Marchese, H.G., 1975. Relación entre la tectonosedimentación, litología y mineralogía de arcillas del Complejo Buenos Aires y la Formación La Tinta (Prov. de Buenos Aires). Revista de la Asociación Argentina de Mineralogía, Petrología y Sedimentología 5 (3–4), 45–58.

Frisicale, M.C., Dimieri, L.V., Dristas, J.A., 2001. Microestructuras en las rocas miloníticas del Cerro El Peregrino, Tandilia. In: Avances en Microtectónica, Asociación Geológica Argentina, Serie D: Publicación Especial N8, vol. 5, pp. 107–111.

Frisicale, M.C., Martínez, F.J., Dimieri, L.V., Dristas, J.A., 2005. Microstructural analysis and *P–T* conditions of the Azul megashear zone, Tandilia, Buenos Aires Province, Argentina. Journal of South American Earth Sciences 19, 433–444.

Frisicale, M.C., Dimieri, L., Araujo, V., Dristas, J., 2010. Mecanismos de deformación en la transición milonitas/*striped gneiss* y milonitas/ultramilonitas en las Sierras de Azul, cratón del Río de la Plata, Buenos Aires. Revista de la Asociación Geológica Argentina 67, 4–18.

Frisicale, M.C., Dimieri, L., Dristas, J.A., Araujo, V., Fortunatti, N., 2012. Microstructural and geochemical analysis of Paleoproterozoic pseudotachylytes in Río de la Plata Craton, Tandilia Belt, Argentina. Geologica Acta 10 (1), 1–8.

Hartmann, L.A., 1998. Deepest exposed crust of Brazil – geochemistry of Paleoproterozoic depleted Santa Maria Chico granulites. Gondwana Research 1, 331–341.

Hartmann, L.A., Santos, J.O.S., Cingolani, C.A., McNaughton, N.J., 2002. Two Paleoproterozoic orogenies in the evolution of the Tandilia Belt, Buenos Aires, as evidenced by zircon U–Pb SHRIMP geochronology. International Geology Review 44, 528–543.

Hartmann, L.A., Bitencourt, M.F., Santos, J.O.S., McNaughton, N.J., Butori Rivera, C., Betiollo, L., 2003. Prolonged Paleoproterozoic magmatic participation in the

Neoproterozoic Dom Feliciano belt, Santa Catarina, Brazil, based on zircon U–Pb SHRIMP geochronology. Journal of South American Earth Sciences 16, 477–492.
Holland, T.J.B., Powell, R., 1996. Thermodynamics of order-disorder in minerals. 2. Symmetric formalism applied to solid solutions. American Mineralogist 81, 1425–1437.
Holland, T.J.B., Powell, R., 1998. An internally consistent thermodynamic data set for phases of petrological interest. Journal of Metamorphic Geology 16, 309–343.
Iacumin, M., Piccirillo, E.M., Girardi, V.A.V., Teixeira, W., Bellieni, G., Echeveste, H., Fernández, R., Pinese, J.P.P., Ribot, A., 2001. Early Proterozoic calc-alkaline and Middle Proterozoic tholeiitic dyke swarms from central-eastern Argentina: petrology, geochemistry, Sr–Nd isotopes and tectonic implications. Journal of Petrology 42, 2109–2143.
Iñiguez, A.M., 1999. La cobertura sedimentaria de Tandilia. In: Caminos, R. (Ed.), Geología Argentina. Servicio Geológico Minero Argentino, Anales, vol. 29, pp. 101–106.
Iñiguez, A.M., Del Valle, A., Poiré, D., Spalletti, L., Zalba, P., 1989. Cuenca Precámbrica-Paleozoico inferior de Tandilia, Provincia de Buenos Aires. In: Chebli, G., Spalletti, L.A. (Eds.), 1989. Cuencas Sedimentarias Argentinas, vol. 6. Instituto Superior de Correlación Geológica, Universidad Nacional de Tucumán, Serie Correlación Geológica, pp. 245–263.
Jercinovic, M.J., Williams, M.L., 2005. Analytical perils (and progress) in electron microprobe trace element analysis applied to geochronology: background acquisition interferences, and beam irradiation effects. American Mineralogist 90, 526–546.
Kleemann, U., Reinhardt, J., 1994. Garnet-biotite thermometry revisited: the effect of Al^{VI} and Ti in biotite. European Journal of Mineralogy 6, 925–941.
Kostadinoff, J., 1995. Geofísica de las Sierras del Sistema de Tandil. Unpubl.. Ph.D. thesis, Facultad de Ciencias Astronomicas y Geofisicas, Universidad Nacional de La Plata, Argentina, pp. 1–178.
Kröner, A., Cordani, U., 2003. African, southern Indian and South American cratons were not part of the Rodinia supercontinent: evidence from field relationships and geochronology. Tectonophysics 375, 325–332.
Leveratto, M.A., Marchese, H.G., 1983. Geología y estratigrafía de la Formación La Tinta (y homólogas) en el rea clave de Sierra de la Tinta-Barker-Villa Cacique-Arroyo Calaveras, prov. de Buenos Aires. Revista de la Asociación Geológica Argentina 38, 235–247.
Liu, Y., Siebel, W., Theye, T., Massonne, H.-J., 2011. Isotopic and structural constraints on the late Miocene to Pliocene evolution of the Namche Barwa area, eastern Himalayan syntaxis, SE Tibet. Gondwana Research 19, 894–909.
Marchese, H., Di Paola, E., 1975. Reinterpretación estratigráfica de la perforación de Punta Mogotes I, Provincia de Buenos Aires. Revista de la Asociación Geológica Argentina 30, 44–52.
Martin, L.A.J., Ballèvre, M., Boulvais, P., Halfpenny, A., Vanderhaeghe, O., Duchêne, S., Deloule, E., 2011. Garnet re-equilibration by coupled dissolution-reprecipitation: evidence from textural, major element and oxygen isotope zoning of 'cloudy' garnet. Journal of Metamorphic Geology 29, 213–232.
Massonne, H.-J., 2004. Ultra high pressure metamorphism. In: Selley, R.C., Cocks, L.R.M., Plimer, I.R. (Eds.), 2004. Encyclopedia of Geology, vol. 5, pp. 533–540.
Massonne, H.-J., 2010. Phase relations and dehydration behaviour of calcareous sediments at very-low to low grade metamorphic conditions. Periodico di Mineralogia 79 (2), 21–43.
Massonne, H.-J., 2011. Pre-conference excursion guide part I: stops 1-1-2-2, German part of the Saxonian Erzgebirge. Geolines 23, 29–59.
Massonne, H.-J., Szpurka, Z., 1997. Thermodynamic properties of white micas on the basis of high-pressure experiments in the systems K_2O–MgO–Al_2O_3–SiO_2–H_2O and K_2O–FeO–Al_2O_3–SiO_2–H_2O. Lithos 41, 229–250.
Massonne, H.-J., Tikovsky, T., Hartmann, L.A., 2001. Petrology of the 2.0 Ga old Santa Maria Chico granulites in southern Rio Grande do Sul, Brazil, and implications for crustal thickening in Paleoproterozoic times. In: XI Congreso Latinoamericano, Montevideo 2001, Report, 4 pp. on CD.
Massonne, H.-J., Kennedy, A., Nasdala, L., Theye, T., 2007. Dating of zircon and monazite from diamondiferous quartzofeldspathic rocks of the Saxonian Erzgebirge. Mineralogical Magazine 71, 407–425.
Massonne, H.-J., Willner, A.P., 2008. Dehydration behaviour of metapelites and mid-ocean ridge basalt at very-low to low grade metamorphic conditions. European Journal of Mineralogy 20, 867–879.
Massonne, H.-J., Clarke, D.B., MacDonald, M.A., 2010. Intrusion level of the Musquodoboit batholith in Nova Scotia, Canada – a case study. Zeitschrift für Geologische Wissenschaften 38, 181–194.
Moyen, J.-F., Stevens, G., 2006. Experimental constraints on TTG petrogenesis: implications for Archean geodynamics. In: Benn, K., Mareschal, J.-C., Condie, K. (Eds.), Archean Geodynamics and Environments. Geophysical Monograph Series, vol. 164, pp. 149–175.
Oyhantçabal, P., Siegesmund, S., Wemmer, K., 2011. The Río de la Plata Craton: a review of units, boundaries, ages and isotopic signatures. International Journal of Earth Sciences 100, 201–220.
Pankhurst, R.J., Ramos, V.A., Linares, E., 2003. Antiquity of the Río de la Plata Craton in Tandilia, southern Buenos Aires Province, Argentina. Journal of South American Earth Sciences 16, 5–13.
Poiré, D.G., Spalletti, L.A., 2005. La cubierta sedimentaria Precámbrica-Paleozoica inferior del Sistema de Tandilla. In: Barrio, R.E., Etcheverry, R.O., Caballé, M.F., Llambías, E. (Eds.), 2005. VI Congreso Geológico Argentino (Relatorio) and Geología y Recursos Minerales de la Provincia de Buenos Aires, 1(5), pp. 51–68. La Plata, Argentina.
Powell, R., Holland, T.J.B., 1999. Relating formulations of the thermodynamics of mineral solid solutions: activity modeling of pyroxenes, amphiboles and micas. American Mineralogist 84, 1–14.
Pyle, J.M., Spear, F.S., Wark, D.A., Daniel, C.G., Storm, L.C., 2005. Contributions to precision and accuracy of chemical ages of monazite. American Mineralogist 90, 547–577.
Ramos, V.A., Leguizamón, A., Kay, S.M., Teruggi, M., 1990. Evolución tectónica de las Sierras de Tandil (Provincia de Buenos Aires). In: XI Congreso Geológico Argentino, San Juan, Actas, vol. 2, pp. 357–360.
Ramos, V.A., 1999. Rasgos estructurales del territorio argentino. 1. Evolución Tectónica de la Argentina. In: Caminos, R. (Ed.), 1999. Geología Argentina, Anales 29, vol. 24. Instituto de Geología y Recursos Minerales, Subsecretaría de Minería, Buenos Aires, pp. 715–784.
Rapela, C.W., Pankhurst, R.J., Casquet, C., Fanning, C.M., Baldo, E.G., González-Casado, J.M., Galindo, C., Dahlquist, J., 2007. The Río de la Plata Craton and the assembly of SW Gondwana. Earth-Science Reviews 83, 49–82.
Rapela, C.W., Fanning, M., Casquet, C., Pankhurst, R.J., Spalletti, L., Poiré, D., Baldo, E.G., 2011. The Río de la Plata Craton and the adjoining Pan-African/Brasiliano terranes: their origins and incorporation into south-west Gondwana. Gondwana Research 20, 673–690.
Reed, S.J.B., Buckley, A., 1998. Rare-earth element determination in minerals by electron-probe microanalysis: application of spectrum synthesis. Mineralogical Magazine 62, 1–8.
Rollinson, H., 2010. Coupled evolution of Archean continental crust and subcontinental lithospheric mantle. Geology 38, 1083–1086.
Rudnick, R.L., 1995. Making continental crust. Nature 378, 571–578.
Scherrer, N.C., Engi, M., Gnos, E., Jakob, V., Liechti, A., 2000. Monazite analysis; from sample preparation to microprobe age dating and REE quantification. Schweizerische Mineralogische und Petrographische Mitteilungen 80, 93–105.
Shchipansky, A.A., Khodorevskaya, L.I., Slabunov, A.I., 2012. The geochemistry and isotopic age of eclogites from the Belomorian Belt (Kola Peninsula): evidence for subducted Archean oceanic crust. Russian Geology and Geophysics 53, 262–280.
Stern, R.J., 2008. Modern-style plate tectonics began in Neoproterozoic time: an alternative interpretation of Earth's tectonic history. In: Condie, K., Pease, V. (Eds.), When Did Plate Tectonics Begin on Planet Earth?. Geological Society of America Special Paper, vol. 440, pp. 265–280.
Texeira, W., Renne, P.R., Bossi, J., Campal, N., D'Agrella Filho, M.S., 1999. ^{40}Ar–^{39}Ar and Rb–Sr geochronology of the Uruguayan dike swarm, Rio de la Plata Craton and implications for Proterozoic intraplate activity in western Gondwana. Precambrian Research 93, 153–180.
Texeira, W., Pinese, J., Iacumin, M., Girardi, V., Piccirillo, E., Echeveste, H., Ribot, A., Fernandez, R., Renne, P., Heaman, L., 2002. Geochronology of calc-alkaline and tholeiitic dyke swarms of Tandilia, Río de la Plata Craton, and their role in the Paleoproterozoic tectonics. In: 3rd South American Symposium on Isotope Geology, Pucón, Chile, Actas, pp. 257–260.
Teruggi, M.E., Kilmurray, J.O., Dalla Salda, L., 1974. Los dominios tectónicos de la región de Balcarce. Revista de la Asociación Geológica Argentina 29, 265–276.
Teruggi, M.E., Leguizamón, M.A., Ramos, V.A., 1988. Metamorfitas de bajo grado con afinidades oceánicas en el basamento de Tandil: su implicancia geotectónica, Provincia de Buenos Aires. Revista de la Asociación Geológica Argentina 43 (3), 366–374.
Tohver, E., Cawood, P.A., Rossello, E.A., Jourdan, F., 2012. Closure of the Clymene Ocean and formation of West Gondwana in the Cambrian: Evidence from the Sierras Australes of the southernmost Rio de la Plata craton, Argentina. Gondwana Research 21, 394–405.
White, R.W., Powell, R., Holland, T.J.B., 2001. Calculation of partial melting equilibria in the system Na_2O–CaO–K_2O–FeO–MgO–Al_2O_3–SiO_2–H_2O (NCKFMASH). Journal of Metamorphic Geology 19, 139–153.
White, R.W., Powell, R., Clarke, G.L., 2003. Prograde metamorphic assemblage evolution during partial melting of metasedimentary rocks at low pressures: migmatites from Mt Stafford, Central Australia. Journal of Petrology 44, 1937–1960.